Influence of Ball Milling Duration on Physicochemical Properties and Compressibility of Calcium Powder Derived from Snail Shells (Achatina fulica)

Puspitasari, Poppy
Department of Mechanical and Industrial Engineering, Universitas Negeri Malang

Triaditama, Bobby
Department of Mechanical and Industrial Engineering, Universitas Negeri Malang

Diki Dwi Pramono
Department of Mechanical and Industrial Engineering, Universitas Negeri Malang

Andriyana, Andri
Department of Mechanical Engineering, Universiti Malaya

https://doi.org/10.5109/7236828

出版情報：Evergreen. 11 (3), pp.1763-1769, 2024-09. 九州大学グリーンテクノロジー研究教育センター
バージョン：

Influence of Ball Milling Duration on Physicochemical Properties and Compressibility of Calcium Powder Derived from Snail Shells (*Achatina fulica*)

Poppy Puspitasari[1,2,*], Bobby Triaditama[1], Diki Dwi Pramono[1], Andri Andriyana[3]

[1]Department of Mechanical and Industrial Engineering, Universitas Negeri Malang, Indonesia

[2]Centre of Advanced Materials and Renewable Energy, Universitas Negeri Malang, Indonesia

[3]Department of Mechanical Engineering, Universiti Malaya, Malaysia

*Author to whom correspondence should be addressed:
E-mail: poppy@um.ac.id

(Received December 21, 2023: Revised June 24, 2024: Accepted August 16, 2024).

Abstract: Ball milling duration has an important role in the synthesis of calcium nanoparticles. The duration of this process can influence the properties of the calcium powder. This study investigates the influence of ball milling duration on the physicochemical properties and compressibility of snail shell powder. Morphology of the samples shows agglomeration with irregular shape. The elemental composition of samples mostly calcium (Ca). The phases formed in the samples are $Ca(OH)_2$, the smallest crystallite size of 21.11 nm. The observed functional groups result shown C-O vibrations of the CO_3^{2-}carbonate group, Ca-O bonds. The compressibility test shows that the sample with 9 hours milling time has the largest compressibility. Based on the research conducted, it shows that milling time has an influence on the properties of snail shell powder.

Keywords: Physicochemical Properties; Compressibility; Snail Shell; Milling Time

1. Introduction

The production of calcium powder from natural source waste is gaining significant attention due to its potential applications in various fields, including renewable energy and environmental sustainability[1)]. One crucial step in this process is the ball milling duration, which significantly impacts the final properties of the calcium powder [2)]. Ball milling is a mechanical process that involves grinding the snail shell into a fine powder. The duration of this process can influence the particle size distribution, crystallinity, and chemical composition of the resulting calcium powder[3)].

Ball milling duration has an important role in the synthesis of calcium oxide (CaO) nanoparticles. The duration of the milling process significantly impacts the size and distribution of the particles, as well as the crystallinity and surface state of the material[4)]. For instance, studies have shown that longer milling times can lead to a decrease in the degree of crystallinity and the formation of fibrous morphologies rather than particulates. The optimal milling time depends on the specific application and the desired properties of the final product[5)]. In the synthesis of CaO nanoparticles from eggshells, the milling time was varied to observe the difference on the size of the produced particle. SEM images revealed that the smallest average particle diameter was achieved by 20 hours of milling, indicating the importance of controlling the milling time to achieve the desired particle size distribution[2)].

The importance of ball milling time is further highlighted by the effects it has on the microstructure and thermal properties of materials. The longer milling times can lead to a broader particle size distribution, which can result in varying thermal properties[6)]. In the synthesis of CaO from by-product calcium sulfate, the milling time was found to influence the reaction mechanism and the resulting product properties. The optimal milling time was determined to be 40 minutes, which resulted in the highest yield of CaO. Therefore, controlling the milling time is essential to achieve the desired properties and to avoid unwanted effects such as agglomeration[7)]. A study on the characterization of nanocrystalline and amorphous calcium carbonate from waste seashells found that the morphology of the powders obtained after different milling times influenced the content of amorphous calcium carbonate (ACC) in the final product. The study concluded that a longer milling time (6 hours) produced a higher content of ACC, which is important for achieving specific properties in the final product[8)]. Overall, the ball milling duration is a critical parameter that must be carefully controlled to achieve the desired properties in calcium powder.

Therefore, this study was conducted to analyse the

effect of ball milling time of 3, 6, and 9 hours on the physicochemical properties and compressibility of calcium powder made from snail shell (*Achatina fulica*).

2. Materials and Methods

This study used snail shells (Achatina fulica) obtained from a local restaurant in Blitar Regency, Indonesia. The snail shells that have been obtained are washed and dried, after drying the snail shells are mechanically crushed so that they are micro-sized, 300g of snail shells were mixed with 100ml of acetone and ball milled with a planetary ball mill (MTI QM-3SP2)[9]. The milling process was performed using time variations of 3, 6, and 9 hours. Then, the samples were dried at 110° C for one hour[10], followed by crushing for one hour[11]. In the next stage, the samples were calcinated at 1000° C (RMF Quartech 2800) for one hour[12,13]. The crushing was repeated again for one hour[11]. The prepared samples were characterized to ascertain the morphology using Scanning Electron Microscopy - Energy Dispersive X-ray Spectroscopy (SEM-EDX), FEI Inspect-S50[14], the samples surface was covered with a layer of gold to increasethe sample'sconductivity prior to observation and the magnification is 100000×, SEM results were analysed using ImageJ software to determine the particle size of the snail shell powder samples. X-Ray Diffraction (XRD), PANalytical E'xpert Pro used to characterize phase and crystallite size[15], the diffraction angle used for the scanning ranged between 10º and 90º at wavelength 1.5406 Å. Fourier Transform Infrared (FTIR) Shimadzu IR Prestige21 used to characterize the functional groups[16], spectra were obtained over a range of 4000-400 cm^{-1}. While the compressibility test was carried out in accordance with ASTM B331-16, the snail shell powder was placed in a SS316 mould and loaded with 1000 kgf and 2000 kgf for 90 seconds using a Universal Testing Machine (ILE IL-904)[17].

3. Result and Discussion

The samples were coded as (SCB), which stood for snail shell (*Achatina fulica*) powder, followed by the number indicating their milling time at the unit of hours.

3.1 Morphology of Snail Shell Powder

Based on Figure 1 SEM results of snail shell powder samples, agglomeration occurs. The measurement results using ImageJ software show that Samples SCB-3, SCB-6 and SCB-9 have an average particle size of 123.24 nm, 76.19 nm and 66.12 nm, as presented in Fig. 1.

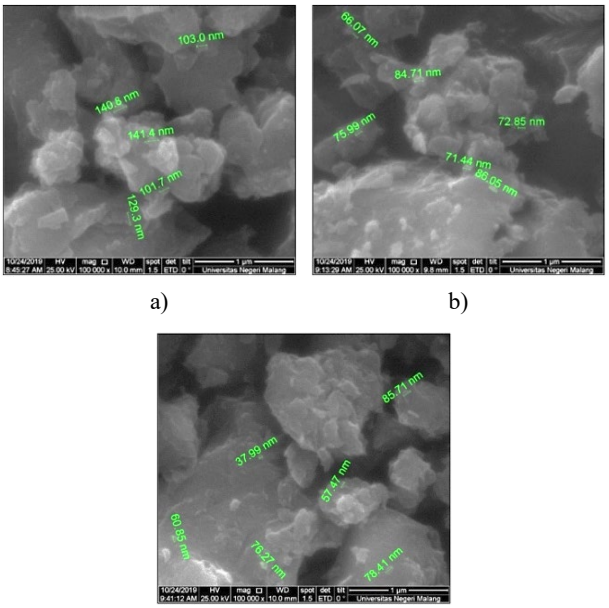

a) b)

c)

Fig. 1: Results of SEM test at 100.000x magnification for SCB-3 sample, b) SCB-6 sample, and c) SCB-9 sample

The three test results exhibit a similarity, specifically in the aggregated irregular shape of the grain[18]. The average grain size becomes smaller with increasing milling time, albeit not significantly. This reduction of size and enhancement of grain fineness are attributed to the ball milling mechanism[15]. The ball mill and the vial or milling cup possess a centrifugal force along their axes, while the milling cup and the bearing plate or rotating disc rotates in the opposite direction, resulting in alternating centrifugal forces and creating a balanced force. This balanced force is achieved through the counterweight combined with the bearing plate, generating frictional force and impact load[19].

The morphology obtained from the sample is agglomeration in the snail shell powder sample. This result is caused by the calcination process, a study by Puspitasari et al., stated that heat treatment or calcination can cause agglomeration in samples, agglomeration observed in samples can increase grain size and potentially contribute to the enlargement of crystallite size[10]. The calcination process results in thermal decomposition and the release of carbon dioxide, besides the application of heat causes the crystals in the grains to enlarge or growth[20]. The calcination process is very influential on the microstructure and morphology of a powder, because during calcination it causes the particles to become united so as to make the density increase (agglomeration), during this process grain boundaries are formed which is the initial stage of recrystallisation and besides that there will also be gas that evaporates[21].

3.2 Elemental Content of Snail Shell Powder

EDX characterisation was carried out to identify the elemental composition of the snail shell powder sample

which aims to analyse the purity of the sample. The results of EDX characterisation are shown in Fig. 2 and table 1.

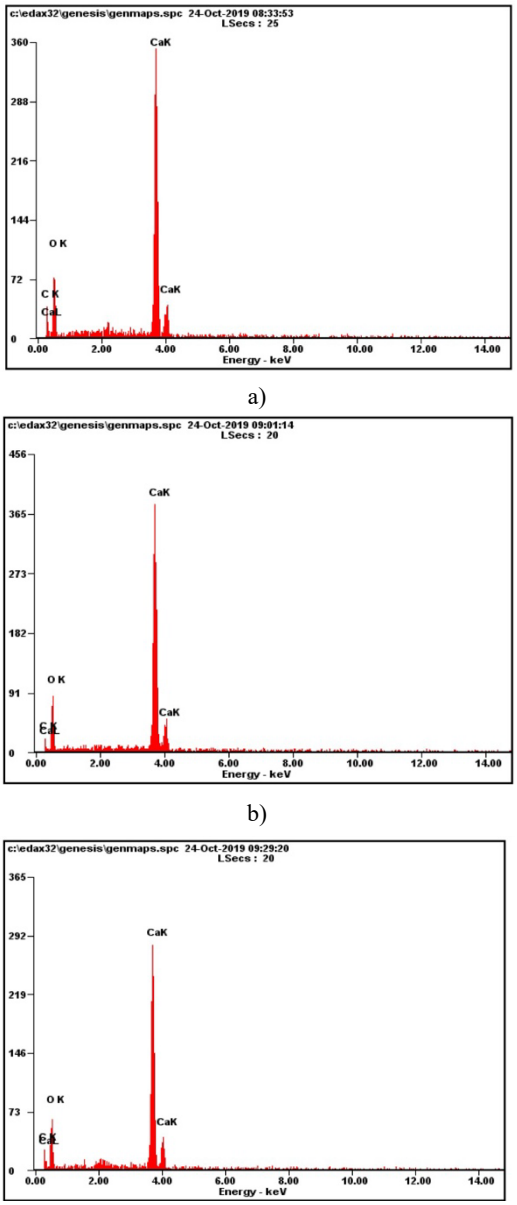

Fig. 2: Spectra EDX of snail shell powder samples.

Table 1. Percentage of constituent elements from the EDX test for snail shell powder samples.

Sample	Element (wt%)		
	Carbon (C)	Oxygen (O)	Calcium (Ca)
SCB-3	6.36	44.89	48.74
SCB-6	2.35	46.65	50.99
SCB-9	2.72	43.84	53.44

The SCB-3 sample presents 6.36 Wt% of carbon (C), followed by 44.89 and 48.74 Wt% of oxygen (O) and calcium (Ca), respectively. Meanwhile, the SCB-6 sample presents 2.35, 46.65, and 50.99 Wt% of carbon (C), oxygen (O), and calcium (Ca), respectively. The last sample, SCB-9, has 2.72, 43.84, and 53.44 Wt% of carbon (C), oxygen (O), and calcium (Ca), respectively.

These test results indicate three central constituent elements from the samples, including carbon (C), oxygen (O), and calcium (Ca). The presence of other elements, such as hydrogen (H), is undetected by the EDX, probably due to their small atomic mass[19]. Besides, fluctuations in the carbon (C) content may arise because of the use of carbon tape in the sample preparation using[19]. Further, the O element content is predominantly observed[19], along with the relatively significant oxygen (O). The accelerated calcium content (Ca) is also identified to be directly proportional to the length of the milling duration. Similarly, Fajri et al (2016) uncovered that the combination of milling time and heat treatment enhances the wt% percentage of calcium content (Ca)[19].

3.3 Phase and Crystall Size of Snail Shell Powder

The XRD results are illustrated in Fig. 3. The obtained Bragg angle, Full Width at Half Maximum (FWHM), intensity peak, and crystal size are presented in Table 2. The crystal size was calculated using the Scherrer Formula in Equation (1)[22,23].

$$d = (K.\lambda)/(\beta \cos \theta) \qquad (1)$$

in which d is the crystal diameter (nm), K represents the constant (0.9)[24,25], λ is the wavelength (1.5406 Å), and β is the Full-Width Half Maximum (FWHM).

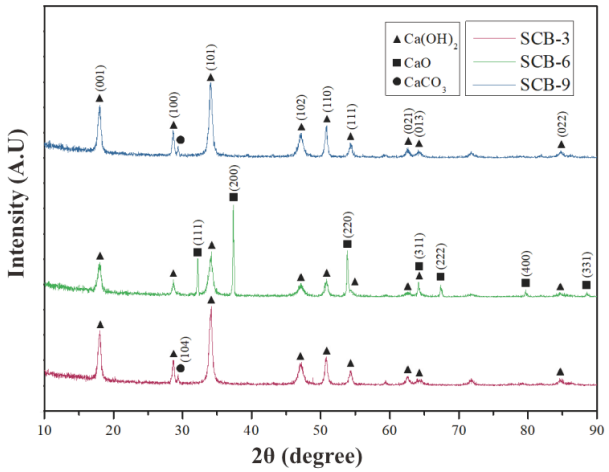

Fig. 3: Diffractogram of XRD results for SCB-3, SCB-6, and SCB-9 samples

Table 1. Crystallite size of SCB-3, SCB-6, and SCB-9 samples

Sample	X-Ray Diffraction		
	Bragg Angle (θ)	FWHM (rad)	Crystallite size (nm)
SCB-3	17.05745	0.006181956	23.46
SCB-6	18.6749	0.001717404	85.22
SCB-9	17.02405	0.006869616	21.11

The XRD test results were analyzed using the Match! (v3.9.0.158) application with a reference database from COD-Inorg REV218120 2019.09.10. The XRD test results indicated that samples SCB-3 and SCB-9 have several peaks, namely [001], [100], [101], [102], [110], [111], [021], [013], and [022], which correspond to the portlandite phase from the $Ca(OH)_2$ compound with a trigonal crystal system (hexagonal axes). The highest peak was observed at 34.1149°. Another peak in samples SCB-3 and SCB-9 appeared at 29.3° with the index [104], corresponding to the calcite phase from the compound of $CaCO_3$ with a trigonal crystal system (hexagonal axes). The XRD analysis results of the SCB-6 sample indicated several peaks, including [111], [200], [220], [311], [222], [400], and [331], matching the lime phase from the CaO compound with a cubic crystal system. Further, the highest peak was identified at 37.3490°.

The transformation of the CaO compound to $Ca(OH)_2$ can be attributed to the reaction with water vapor in the air[26,27]. Conversely, the occurrence of a limited quantity of $CaCO_3$ compound can be attributed to the presence of residual compounds that did not undergo complete conversion into CaO during the heat treatment procedure[26]. Besides, the minimum $CaCO_3$ content can also be caused by the reaction of $Ca(OH)_2$ with CO_2 in the air[28,29].

3.4 Functional Groups of Snail Shell Powder

The functional groups of Achatina fulica snail shell powder were analyzed using FTIR spectroscopy. The FTIR test results are illustrated in Fig. 4.

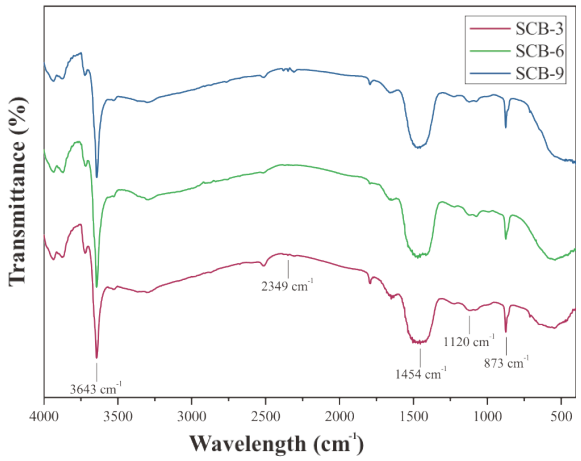

Fig. 4: FTIR test results for snail shell powder samples

Based on the results of the X-ray diffraction (XRD) test, the compounds present in the Achatina fulica snail shell powder with variations of 3, 6, and 9 hours milling times are $Ca(OH)_2$. The results presented in Fig.5.4 suggest no significant differences from the samples, so the three samples are similar. A study presented by Khachani et al (2014) described that the FTIR of synthesized $Ca(OH)_2$ shows a shallow absorption band at 3642 cm^{-1} due to the O-H stretching[30]. The absorption at 1464, 1080, and 873 cm^{-1} represent the different vibrations of C-O from the CO_3^{2-} carbonate group. Additionally, we observed a slight decrease in the spectrum at 2352 cm^{-1} due to the presence of CO_2 gas[31]. The emergence of the carbonate group also represents the contaminant within the CO_2 sample. Other studies also show relevant findings. The O-H stretching bond from hydroxide also presents the bonds of $Ca(OH)_2$ at around 3628-3649 cm^{-1} wavenumber[27,28,30,32–35]. The vibration at around 1417-1464, 1041-1091, and 713-924 cm^{-1} suggest various C-O vibrations from CO_3^{2-}[26–28,30,32,34]. The Ca-O vibration was detected at the 393-875 cm^{-1} wavenumber[27,28,32,35].

3.5 Compressibility of Snail Shell Powder

The compressibility test was carried out on Achatina fulica snail shell samples. The tapped density values were calculated using Equation (2)[36].

$$\rho = m/V_{tapped} \qquad (2)$$

In which ρ is the tapped density (g/cm^3), m represents the solid mass (g), and V is the tapped volume (cm^3). The compressive ratio was calculated using Formula (3)[37].

$$CR = ((h_0 - h_p)/h_0) \times 100 \quad (3)$$

Where CR shows the compressive ratio (%), h_0 is the height at *zero pressure* (mm), and h_p is the solid height (mm). The compressibility was calculated using Formula (4)[38].

$$\beta_c = -1/V\,(\partial_V/\partial_P) \qquad (4)$$

Where β represents the compressibility value (m^2/N or Pa^{-1}), V is the initial volume (m^3), ∂_V is the difference in volume before and after applying pressure (m^3), and ∂_P is the difference in pressure before and after applying pressure (N/m^2 atau Pa). The value of the compression modulus was calculated using Equation (5)[39].

$$K_c = -V(\partial_P/\partial_V) \quad (5)$$

Where K_c represents the compression modulus value (N/m^2 atau Pa), V is the initial volume (m^3), ∂_P the difference in pressure before and after applying pressure (N/m^2 atau Pa), and ∂_V is the difference in volume before and after applying pressure (m^3).

The results of density, compression ratio, compressibility, and compression modulus tests are illustrated in Fig. 5.

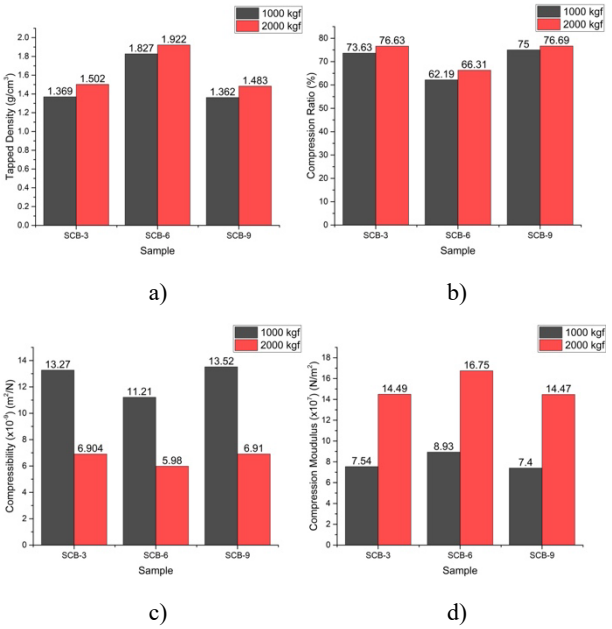

Fig. 5: Histogram a) tapped density, b) compression ratio, c) compressibility and d) compression moudulus of snail shell powder samples.

The data presented in Figure 5 a), and b), showed that with a load of 2000 kgf, the obtained density and compression ratio are higher than from the load of 1000 kgf. This increase can be attributed to the dwelling time of 90 seconds. The progression of material density may be induced by dynamic loading, where a specific dwelling time is applied[17].

In addition, the data shown in Figure 5 c) and d) showed that signify that the samples have lower compressibility at 2000 kgf than the compressibility at 1000 kgf loading. In contrast, the compression modulus for a load of 2000 kgf is higher than that under a load of 1000 kgf. This aligns with the correlation indicated by the compression modulus equation, which is the reciprocal of the Equation for the modulus of compression[38,39].

In general, the garnered data indicate the effects of crystallite size on the density, compression ratio, compressibility, and compression modulus. The largest crystallite size of 85.22 nm was observed in the SCB-6 sample, followed by the SCB-3 sample, with a size of 23.46 nm, while the smallest size of 21.11 nm was found in the SCB-9 sample. The larger crystallite size is directly proportional to larger density values, but it is inversely proportional to the compression ratio, as illustrated in Table 4. The greater crystallite size leads to lower compressibility values, yet it is inversely proportional to the compression modulus[29].

The calculated compression ratio results align with the study from Yu et al (2020), reporting that a high compression ratio represents better compressibility of the sample[37]. Similarly, Hamad et al (2015) uncovered that finer and smaller particles tend to fill the gaps between larger particles, resulting in higher compressibility[40]. Meanwhile, Oikonomou et al (2013) asserted that better particle size enhances the compressibility of the powder[41].

4. Conclusion

The morphology of the snail shell powder sample shows agglomeration with irregular grain shape, the average grain size decreases with increasing ball milling time. The elemental composition of snail shell powder is mostly calcium (Ca) and oxygen (O), and there is carbon (C) content in the sample. The phases formed in the snail shell powder sample are $Ca(OH)_2$, $CaCO_3$ and CaO, in the 9-hour milling time sample has the smallest crystallite size of 21.11 nm. The observed functional groups include O-H stretching, various C-O vibrations of the CO_3^{2-} carbonate group, Ca-O bonds. The compressibility test shows that the sample with 9 hours milling time has the largest compressibility. Based on the research conducted, it shows that milling time has an influence on the morphology, elemental content, phases formed, crystallite size and compressibility of snail shell powder.

Acknowledgements

Author would like to thank the State University of Malang.

Nomenclature

d	crystallite size (nm)
K	constant (0.9)
λ	wavelength (1.5406 Å)
β	Full-Width Half Maximum (rad)
θ	bragg angle (°)
ρ	tapped density (g/cm^3)
m	solid mass (g)
V_{tapped}	tapped volume (cm^3)
CR	compression ratio (%)
h_0	height at *zero pressure* (mm)
h_p	solid height (mm)
β_c	compressibility value (m^2/N or Pa^{-1}),
V	initial volume (m^3)
∂_V	difference in volume before and after applying pressure (m^3)
∂_P	difference in pressure before and after applying pressure (N/m^2 atau Pa)
K_c	compression modulus value (N/ m^2 atau Pa)

References

1) L.K. Wei, S.Z. Abd Rahim, M.M. Al Bakri Abdullah, A.T.M. Yin, M.F. Ghazali, M.F. Omar, O. Nemeș, A.V. Sandu, P. Vizureanu, and A.E. hadj Abdellah, "Producing metal powder from machining chips using ball milling process: a review," *Materials*

(Basel)., **16** (*13*) (2023). doi:10.3390/ma16134635.
2) M. Baláž, "Ball milling of eggshell waste as a green and sustainable approach: a review," *Adv. Colloid Interface Sci.*, **256** 256–275 (2018). doi:10.1016/j.cis.2018.04.001.
3) F. Granados-Correa, J. Bonifacio-Martínez, and J. Serrano-Gómez, "The ball milling effect on tribasic calcium phosphate and its chromium (vi) ion sorption properties," *J. Chil. Chem. Soc.*, **54** (*3*) 252–255 (2009). doi:10.4067/S0717-97072009000300010.
4) R.P. Pahune, V.J. Jaiswal, O. V Tekade, V. V Kale, and M.J. Umekar, "Sustainable sources and extraction methods of calcium for expanding dietary supplement sector journal of chemical health risks," *J. Chem. Heal. Risks*, **14** 461–473 (2024).
5) K. Wahyuningsih, Jumeri, and Wagiman, "Optimization of production process of nano-calcium oxide from pinctada maxima shell by using taguchi method," *Indones. J. Chem.*, **19** (*2*) 356–367 (2019). doi:10.22146/ijc.33871.
6) N. Le Bolay, "On agglomeration phenomena in ball mills: application to the synthesis of composite materials," *Powder Technol.*, **130** (*1–3*) 450–455 (2003). doi:10.1016/S0032-5910(02)00249-8.
7) L. Wu, Z. Tao, Z.M. Zhao, W.A. Ghafar, Y. Tao, S. Liao, and Y. Zhang, "Effect of ball milling time on the performance of phosphorous building gypsum," *Adv. Civ. Eng.*, **2022** (2022). doi:10.1155/2022/7670057.
8) C. Marchini, C. Triunfo, N. Greggio, S. Fermani, D. Montroni, A. Migliori, A. Gradone, S. Goffredo, G. Maoloni, J. Gómez Morales, H. Cölfen, and G. Falini, "Nanocrystalline and amorphous calcium carbonate from waste seashells by ball milling mechanochemistry processes," *Cryst. Growth Des.*, **24** (*2*) 657–668 (2024). doi:10.1021/acs.cgd.3c01007.
9) A.B.D. Nandiyanto, R. Andika, M. Aziz, and L.S. Riza, "Working volume and milling time on the product size/morphology, product yield, and electricity consumption in the ball-milling process of organic material," *Indones. J. Sci. Technol.*, **3** (*2*) 82–94 (2018).
10) P. Puspitasari, V. Yuwanda, Sukarni, and J.W. Dika, "The properties of eggshell powders with the variation of sintering duration," *IOP Conf. Ser. Mater. Sci. Eng.*, **515** (*1*) (2019). doi:10.1088/1757-899X/515/1/012104.
11) N.S. Supriyanto, Sukarni, P. Puspitasari, and A.A. Permanasari, "Synthesis and Characterization of CaO/CaCO3 from Quail Eggshell Waste by Solid State Reaction Process," in: AIP Conf. Proc., AIP Publishing LLC, 2019: p. 040032. doi:10.1063/1.5115670.
12) A. Shavandi, A.E.D.A. Bekhit, A. Ali, and Z. Sun, "Synthesis of nano-hydroxyapatite (nha) from waste mussel shells using a rapid microwave method," *Mater. Chem. Phys.*, **149**–**150** 607–616 (2015).
13) H.F.N. Zhorifah, P. Puspitasari, Andoko, D.I. Tsamroh, and A.A. Permanasari, "Optimization of the Mastication Strength of Hydroxyapatite as an Eggshell-Based Tooth Filler," in: AIP Conf. Proc., 2019: p. 050010. doi:10.1063/1.5115686.
14) H. Suryanto, U. Yanuhar, A.A. Fikri, and G. Mahasri, "Chlorella vulgaris-mediated nanosilver synthesis with chitosan capping agent," *Evergreen*, **10** (*1*) 146–154 (2023). doi:10.5109/6781061.
15) A. Islam, S.P. Dwivedi, V. Kumar Dwivedi, and R. Yadav, "Extraction of Chromium Oxide from CCLW to Develop the Aluminium Based Composite by FSP as Reinforcement alongwith Alumina," 2022.
16) S. Salprima Yudha, C. Banon, R. Pertiwi, D.A. Triawan, and J.I. Han, "Cost-effective synthesis of ceo2-sio2 based on oil palm leaves for the removal of toxic compounds," *Evergreen*, **10** (*3*) 1307–1312 (2023). doi:10.5109/7151676.
17) N. Qosim, P. Murdanto, and P. Puspitasari, "Analisis sifat fisik dan kompresibilitas nanopowder zinc oxide (zno) sebagai alternatif material amalgam," *J. Rekayasa Mesin*, **9** (*1*) 9–14 (2018).
18) A. Razak, N. Mat Isa, S. Kinit, and S. Adzila, "Effect of calcination temperature on the properties of eggshell waste (ew) powder for biomedical application," *Evergr. Jt. J. Nov. Carbon Resour. Sci. Green Asia Strateg.*, **10** (*2*) 782–791 (2023). doi:10.5109/6792828
19) H. Fajri, Gunawarman, J. Affi, and R.S. Putra, "Synthesize and characterization of hydroxyapatite from freshwater snail shell sulcospira sp. proceed by combination of ball milling and heat treatment," *J. Ocean. Mech. Aerosp.*, **37** 9–14 (2016).
20) S.L. Kang, "Sintering: Densification, Grain Growth and Microstructure," 1st ed., Elsevier, British, 2005.
21) G.S. Kumar, A. Ramakrishnan, and Y.-T. Hung, "Lime Calcination," in: L.K. Wang, N.K. Shammas, Y.-T. Hung (Eds.), Adv. Physicochem. Treat. Technol., Humana Press, New Jersey, 2010: pp. 611–633. doi:10.1007/978-1-59745-173-4_14.
22) R.K. Goyal, "Nanomaterials and Nanocomposites," CRC Press, Boca Raton : Taylor & Francis, CRC Press, 2018., 2017. doi:10.1201/9781315153285.
23) P. Poppy, C.S. Putra, A.A. Permanasari, D.D. Pramono, and Andoko, "Physical and Magnetic Properties of Nickel Cobalt Oxide (NiCo2O4) as Synthesized by Self-Combustion Method," in: S.A.A. Karim, P. Puspitasari (Eds.), Adv. Mater. Towar. Energy Sustain., 1st ed., CRC Press, Boca Raton, 2023: pp. 4–31. doi:http://dx.doi.org/10.21203/rs.3.rs-2657087/v1.
24) S. Hussain, and K. Sabiruddin, "Effect of heat treatment on the synthesis of hydroxyapatite from indian clam seashell by hydrothermal method," *Ceram. Int.*, **47** (*21*) 29660–29669 (2021). doi:10.1016/j.ceramint.2021.07.137.
25) D.D. Pramono, and P. Puspitasari, "Comparison of

physicochemical properties of hydroxyapatite from scallop shell synthesized by wet chemical method with and without sonication process Comparison of Physicochemical Properties of Hydroxyapatite from Scallop Shell Synthesized by Wet Chemical Method With and Without Sonication Process," in: Proc. Int. Conf. Green Eng. Technol. 2022 (IConGETech 2022), AIP Conference Proceedings, Arau, 2024: p. 040034. doi:10.1063/5.0199107.

26) A. Lesbani, P. Tamba, R. Mohadi, and F. Fahmariyanti, "Preparation of calcium oxide from achatina fulica as catalyst for production of biodiesel from waste cooking oil," *Indones. J. Chem.*, **13** (*2*) 176–180 (2013). doi:10.22146/ijc.21302.
27) A. Lesbani, S.O. Ceria Sitompul, R. Mohadi, and N. Hidayati, "Characterization and utilization of calcium oxide (cao) thermally decomposed from fish bones as a catalyst in the production of biodiesel from waste cooking oil," *Makara J. Technol.*, **20** (*3*) 121 (2016). doi:10.7454/mst.v20i3.3066.
28) M. Galván-Ruiz, J. Hernández, L. Baños, J. Noriega-Montes, and M.E. Rodríguez-García, "Characterization of calcium carbonate, calcium oxide, and calcium hydroxide as starting point to the improvement of lime for their use in construction," *J. Mater. Civ. Eng.*, **21** (*11*) 694–698 (2009). doi:10.1061/(ASCE)0899-1561(2009)21:11(694).
29) D.D. Pramono, P. Puspitasari, A.A. Permanasari, S. Sukarni, and A. Wahyudiono, "Effect of Sintering Time on Porosity and Compressibility of Calcium Carbonate from Amusium Pleuronectes (Scallop Shell)," in: AIP Conf. Proc., American Institute of Physics Inc., 2023. doi:10.1063/5.0120990.
30) M. Khachani, A. El Hamidi, M. Halim, and S. Arsalane, "Non-isothermal kinetic and thermodynamic studies of the dehydroxylation process of synthetic calcium hydroxide ca(oh)2," *J. Mater. Environ. Sci.*, **5** (*2*) 615–624 (2014).
31) P. Puspitasari, and D.D. Pramono, "Phase Identification, Morphology, and Compressibility of Scallop Shell Powder (Amusium Pleuronectes) for Bone Implant Materials," in: Nanotechnologies Green Chem. Environ. Sustain., CRC Press, Boca Raton, 2022: pp. 5–25. doi:10.1201/9781003320746-2.
32) M. Galvan-Ruiz, L. Baños, and M.E. Rodriguez-Garcia, "Lime characterization as a food additive," *Sens. Instrum. Food Qual. Saf.*, (2007). doi:10.1007/s11694-007-9019-8.
33) Z. Liang, Q. Wang, B. Dong, B. Jiang, and F. Xing, "Ion-triggered calcium hydroxide microcapsules for enhanced corrosion resistance of steel bars," *RSC Adv.*, **8** (*69*) 39536–39544 (2018). doi:10.1039/C8RA07382A.
34) B. Priyadarshini, S. Selvan, K. Narayanan, and A. Fawzy, "Characterization of chlorhexidine-loaded calcium-hydroxide microparticles as a potential dental pulp-capping material," *Bioengineering*, **4** (*4*) 59 (2017). doi:10.3390/bioengineering4030059.
35) N. Tangboriboon, P. Phudkrachang, L. Mulsow, W. Kunchornsup, and A. Sirivat, "Removal of water extractable proteins from concentrated natural rubber latex by eggshells," *J. Elastomers Plast.*, **45** (*3*) 253–269 (2013). doi:10.1177/0095244312452273.
36) O.D. Neikov, and N.A. Yefimov, "Powder Characterization and Testing," in: Handb. Non-Ferrous Met. Powders, Elsevier, 2019: pp. 3–62. doi:10.1016/B978-0-08-100543-9.00001-4.
37) Y. Yu, L. Zhao, X. Lin, Y. Wang, and Y. Feng, "A model to simultaneously evaluate the compressibility and compactibility of a powder based on the compression ratio," *Int. J. Pharm.*, 119023 (2020). doi:10.1016/j.ijpharm.2020.119023.
38) M.J. Moran, H.N. Shapiro, D.D. Boettner, and M.B. Bailey, "Fundamentals of Engineering Thermodynamics," 7th ed., John Wiley & Sons, 2011.
39) C. Kittel, and P. McEuen, "Introduction to Solid State Physics," John Wiley & Sons, 2018.
40) I.M. Hamad, A.M.A. Salman, S. Elkarib, and W.A.M.A. Salman, "The effect of particle size on compressibility of cinnamon granules," *J. Appl. Ind. Sci.*, **3** (*4*) 150–153 (2015).
41) C. Oikonomou, E. Hryha, Å. Ahlin, and L. Nyborg, "Effect of Powder Properties on the Compressibility of Water-Atomized Iron and Low-Alloyed Steel Grades," in: Int. Powder Metall. Congr. Exhib. Euro PM 2013, 2013.